Average neutron energies from separated delayed-neutron precursors*

P. L. Reeder, J. F. Wright,† and L. J. Alquist
Battelle, Pacific Northwest Laboratories, Richland, Washington 99352
(Received 20 September 1976)

Average delayed-neutron energies for 16 isotopes of Br, Rb, I, and Cs have been measured by means of detector ring counting rate ratios in a polyethylene-moderated neutron counter system. An on-line mass spectrometer facility was used to give chemically and mass separated sources of delayed-neutron precursors. A simple expression predicts general trends of the average delayed-neutron energies. Average delayed-neutron energies of individual precursors were weighted by the corresponding delayed-neutron yields and combined to give average energies for all six delayed-neutron groups commonly used in reactor kinetics calculations.

[RADIOACTIVITY ^{87,88,89}Br, ^{92,93,94,95,96,97}Rb, ^{137}I, ^{141,142,143,144,145,146}Cs; measured average delayed-neutron energy; on-line mass separation, polyethylene-moderated neutron counter.]

I. INTRODUCTION

Delayed neutron studies of separated isotopes of Br, Rb, I, and Cs are currently in progress at the spectrometer for on-line analysis of radionuclides (SOLAR) facility operated by Battelle, Pacific Northwest Laboratories at the TRIGA reactor at Washington State University. In this paper we report average delayed-neutron energies measured by detector ring counting rate ratios in a polyethylene-moderated multicounter neutron detector system. In the following paper[1] we report delayed-neutron emission probabilities (P_n) measured with the same neutron detector.

The energy spectra of delayed neutrons are of practical importance in calculations of reactor dynamics. In particular, fast breeder reactors are more sensitive to the details of the delayed-neutron spectra than are thermal reactors.[2,3] Improved proton recoil spectrometers have been used in recent years to obtain delayed-neutron energy spectra from unseparated samples of fission products to provide data of use to reactor designers.[4,5] Similar data have been obtained by use of ^{3}He neutron spectrometers.[6,7] These data all show the presence of discrete lines with intensities dependent on the incident neutron energy and the target nuclide undergoing fission.

Energy spectra of delayed neutrons are also of interest in nuclear spectroscopic studies of very neutron rich nuclides. Delayed neutrons are emitted from neutron unbound levels and thus provide a means for studying the β strength function to highly excited levels in the daughter nuclide.[8] Detailed studies of this type require chemical and/or mass separation of the fission products. Fast radiochemical separations were used by Franz *et al.* to provide sources of ^{85}As and ^{135}Sb for neutron energy measurements.[9] Chrysochoides *et al.* studied the spectrum of ^{87}Br and ^{88}Br using a fast chemical separation and time-of-flight counting.[10] Delayed-neutron energy measurements have also been performed at the on-line isotope separators TRISTAN[11] and particularly at OSIRIS.[8,12-14]

Most of the delayed-neutron energy spectra reported thus far have been for nuclides with half-lives greater than 1 sec for which the fission yields are still fairly large. For precursors with half-lives less than 1 sec, the fission yields drop off rapidly. It will be difficult to obtain sufficient counting rates to measure their energy spectra using current techniques. In this paper we report the measurements of average neutron energies for 16 separated Br, Rb, I, and Cs isotopes including several short-lived, low-yield precursors.

The same theoretical treatments which have been used to predict the energy spectra can easily be modified to predict the average neutron energy.[15] These results should therefore permit comparisons of theory and experiment for nuclides far from stability where β decay energies and neutron energy windows are quite large.

II. EXPERIMENTAL DETAILS

A. SOLAR Facility

The SOLAR facility is an on-line mass spectrometer located at a 1 MW TRIGA reactor at Washington State University. The ^{235}U target and thermal ionization source are mounted in a hole in the thermal column and the ion beams are extracted through a 2.3 m evacuated pipe. Positive ion beams of Rb and Cs and negative ion beams of Br and I are available. A detailed description of the origi-

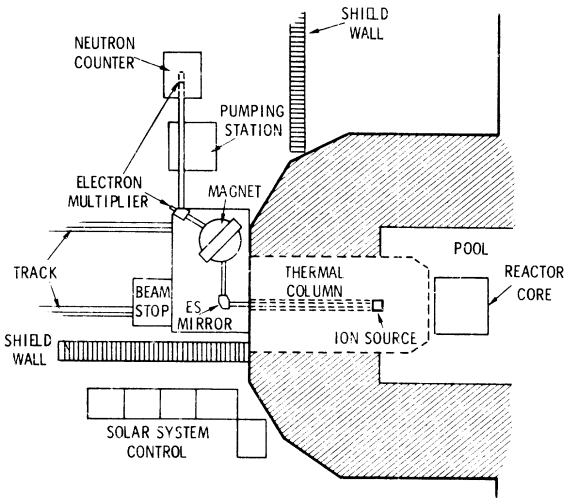

FIG. 1. Floor plan of SOLAR on-line mass spectrometer facility.

nal facility has been published.[16] Since then the facility has been modified by the addition of a 2.3 m beam pipe extension. A single mass ion beam can now be sent to a collection point which is free from interfering radiation from neighboring masses. The revised facility is shown in Fig. 1.

B. SOLAR Neutron Counter (SNC)

The neutron counter used for these measurements was designed to surround an electron multiplier placed at the collection point. The delayed-neutron precursors were deposited on the first dynode of the electron multiplier. This design which was required for the delayed-neutron emission probability experiments described in the following paper permitted simultaneous counting of the ion beam and the delayed neutrons.

The neutron counter consisted of a block of polyethylene $30.5\times30.5\times48.3$ cm^3 in which 42 ^{3}He gas counter tubes were embedded. A central hole (8.97 cm diam) accommodated the ion beam pipe, the electron multiplier, and the multiplier tube base with the voltage divider string. The polyethylene block was shielded on all sides by a sheet of Cd 0.0508 cm thick, 4 boral plates each 0.635 cm thick, and polyethylene 10.16 cm thick. This shielding was penetrated only by a 5.08 cm diam hole for the ion beam pipe and a small hole for 5 high voltage and signal cables.

The 42 counter tubes were arranged in 3 concentric rings about the central beam hole with 9 tubes in the inner ring, 9 tubes in the middle ring, and 24 tubes in the outer ring as shown in Fig. 2. The counter tubes were 2.54 cm diam by 38.1 cm long filled with 8 atm of ^{3}He.[17] The tubes had been previously selected to give equal pulse heights so that many tubes could be connected in parallel and be operated from a single high voltage supply without degrading the pulse height resolution. Each ring of tubes was wired in parallel with a separate preamplifier for each ring. For most of this work, one high voltage power supply was connected to both the middle ring and inner ring preamplifiers (18 tubes) and another high voltage supply was used for the outer ring (24 tubes). Later on, separate high-voltage power supplies were used for each ring. Operating voltages of about +4100 V were used.

The neutron signals from the preamplifiers were amplified, sent through discriminators, and then scaled. Amplifier gains were set by displaying the pulse amplitude on a 100-channel analyzer. The neutron peak (full width at half maximum = 17 channels) was set in channel 90 and the discriminator level was set at channel 50. A typical pulse height spectrum of the inner ring is shown in Fig. 3 for a ^{252}Cf source. The ^{252}Cf source and the delayed neutron sources were relatively free of γ pile-up problems and a distinct valley near channel 20 could be seen between wall-effect neutron pulses and the tail of the γ pile-up pulses. However, the strong photoneutron sources used for calibrations had γ pile-up pulses extending as far as channel 40. The discriminator was therefore set at channel 50 so that the calibration and data runs could all be taken under the same conditions. Separate scalers were used for each ring of tubes in all of the counter efficiency measurements described

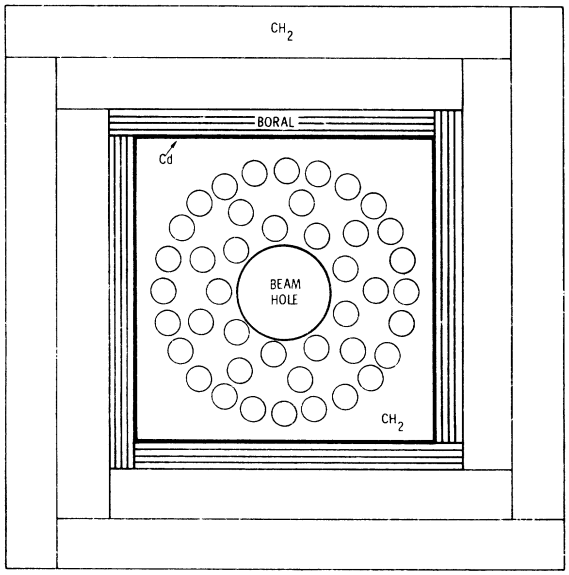

FIG. 2. Diagram of SOLAR neutron counter (SNC). The beam hole radius is 4.48 cm and radii of the counter-rings are 6.35, 8.89, and 12.07 cm, respectively.

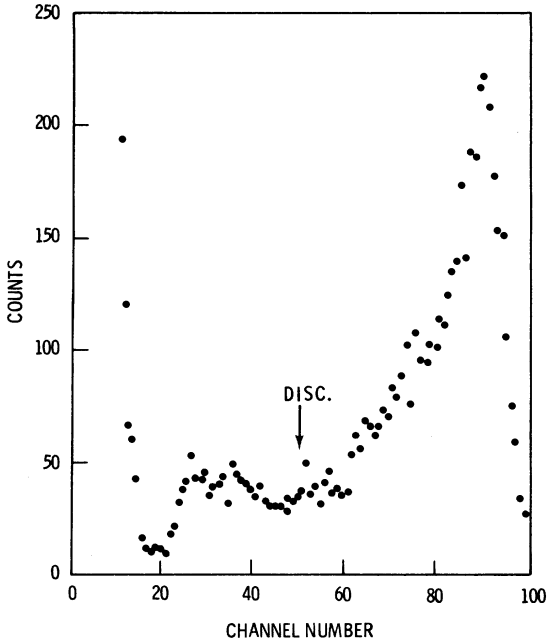

FIG. 3. Typical pulse height spectrum of neutrons from a ^{252}Cf source in inner ring of nine ^{3}He proportional counters connected in parallel.

below. However, many of the ring ratio and P_n data were obtained with the preamplifier outputs from the middle and outer rings tied together and sent to a single scaler.

C. Absolute efficiency of SOLAR neutron counter

The absolute efficiency of each ring of tubes was determined as a function of neutron energy by counting several photoneutron sources and a RaBe source which had been calibrated against a standard ^{252}Cf source. The standard ^{252}Cf source was originally calibrated for Washington State University in 1970 by the Savannah River Laboratory by use of the manganese sulfate bath method to an accuracy of ±3%. Because of the large decay factor needed to correct the source strength to 1976, the ^{252}Cf source was recalibrated at Battelle, Pacific Northwest Laboratory. The ^{252}Cf source was compared with the Hanford Standard PuBe source M1221 [18] by use of the Hanford precision long counter (H4) [19] The new calibration gave the ^{252}Cf neutron emission rate as $(3.47 \pm 0.07)\times 10^5$ n/sec on March 10, 1976. The older calibration corrected to the same date gave a value of $(3.41 \pm 0.10)\times 10^5$ n/sec which is in excellent agreement.

The photoneutron and other sources used to give the energy dependence of the SNC are listed in Table I along with the neutron energies and intensities.

The Hanford precision long counter H4 was used

TABLE I. Neutron sources and energies.

Source	Neutron energy (MeV)	Neutron emission rate (n/sec)
^{124}SbBe	0.024	1.4×10^4
^{24}NaD$_2$O	0.27	3.3×10^3
^{24}NaBe	0.83	1.4×10^3
^{252}Cf	2.35[a]	3.4×10^5
RaBe	3.9[a]	8.2×10^3
PuBe	4.2[a]	1.8×10^6

[a]Average over neutron spectrum.

to calibrate each of the photoneutron sources and the small RaBe source against the ^{252}Cf source. Corrections were made for the room-return neutrons and the slight energy dependence of the long counter. The photoneutron and RaBe sources were then counted in the SNC at the position of the first dynode of the electron multiplier which corresponded to the deposition point of the delayed-neutron precursors. The ^{252}Cf and PuBe sources were too intense to be used inside the SNC so the RaBe source was used to monitor the performance of the counter tubes from day to day. The SNC was calibrated with the photoneutron sources at the beginning of this work and 10 months later at the end of this work. No change in the absolute efficiency of the SNC versus neutron energy was observed.

In Fig. 4 is shown the absolute efficiency of the

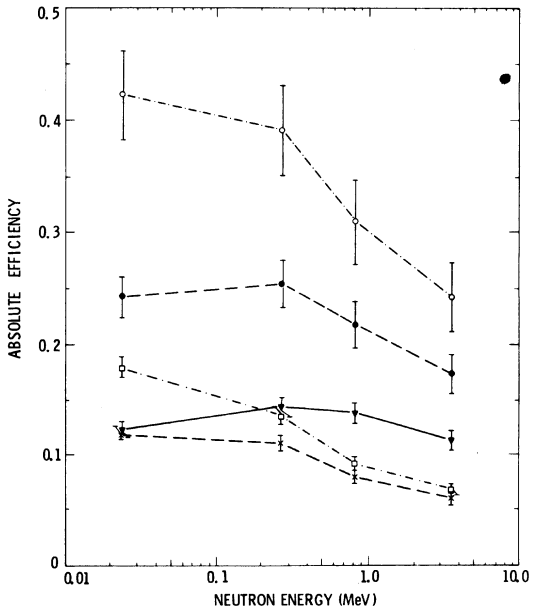

FIG. 4. Absolute efficiency of the SNC versus neutron energy: □, inner ring; ×, middle ring; ▼, outer ring; ●, middle plus outer rings; and ○, all three rings together.

SNC versus neutron energy for each of the three rings, for the middle plus outer rings, and for all three rings together. The inner ring was undermoderated so its efficiency was a strong function of neutron energy. The combined efficiency of the middle plus outer rings was relatively constant at (24.2 ± 2.2)% over the energy range of interest (0.02–0.8 MeV). For this reason, much of the delayed-neutron data was obtained with the middle and outer rings connected to a single scaler.

The errors on the absolute efficiency determinations are primarily due to the large physical dimensions of the photoneutron sources and the uncertainty in positioning the sources with respect to the long counter. Because of low counting rates, the photoneutron sources were counted at a distance of 30 cm from the long counter which meant that the sources were not point sources. Stronger sources could not be used inside the SNC because of γ pile-up problems. The over-all uncertainties in the efficiencies were typically about 7%.

The experimental efficiency curves of Fig. 4 have been compared with calculated response functions for each ring generated by the neutron transport code ONETRAN.[20] The agreement is generally good but detailed comparisons will be presented elsewhere.[21]

D. Calibration of ring ratio versus energy

The use of independent banks of counters embedded in polyethylene to correlate count rate ratios with neutron energies has been discussed previously by East and Walton.[22] If the efficiency versus neutron energy curve of one bank of counters is quite different from the efficiency versus neutron energy curve of another bank of counters, the ratio of counts in the two banks will be a function of neutron energy. Each ring of counters in the SNC could be operated as a bank of counters with distinct efficiency versus energy curves as shown in Fig. 4. In the energy region from 0.024 to 0.8 MeV the outer ring efficiency versus energy curve was relatively flat, whereas the inner and middle rings had decreasing efficiency versus energy curves. When each ring was scaled separately two independent ring ratios were obtained. In particular, the ratios outer/inner and outer/middle were calculated since these ratios showed the greatest dependence on neutron energy. However, since many of the data were obtained using just two scalers, the ratio outer-plus-middle/inner was determined in every case. Calibration curves for each of these three ring ratios versus neutron energy were calculated from the counting data for the photoneutron sources and are shown in Fig. 5 as solid lines. For the ring ratios, the absolute source strength is not needed, so the major uncertainty is simply the statistics of the counting data with the sources inside the SNC.

The photoneutron sources emit monoenergetic neutrons and so the calibration curves based on these points do not accurately represent the calibration curves needed for sources having a spectrum of neutron energies. In order to determine a correction for the delayed neutron spectrum, we proceed as follows. For a monoenergetic source the ring ratio is given by the product of source emission rate N times the counter efficiency for a given ring divided by the source emission rate times the counter efficiency for some other ring. Taking the ratio of outer ring to inner ring as an example, we write

$$\frac{O}{I} = \frac{N\epsilon_O}{N\epsilon_I} = \frac{\epsilon_O}{\epsilon_I}, \tag{1}$$

where O/I is the observed ring ratio, ϵ_O is the efficiency of the outer ring, and ϵ_I is the efficiency of the inner ring. For the SNC, ϵ_O is approximately constant and ϵ_I is a decreasing function of energy, so the ring ratio O/I is a generally increasing function of energy.

For sources with a spectrum of neutron energies, Eq. (1) is modified to give

$$\frac{O}{I} = \frac{\int N(E)\epsilon_O(E)\,dE}{\int N(E)\epsilon_I(E)\,dE}, \tag{2}$$

where $N(E)$ is the neutron intensity as a function of energy and $\epsilon(E)$ is the efficiency of a particular ring as a function of energy. If both the numerator and denominator in Eq. (2) are divided by the total neutron emission rate $N = \int N(E)\,dE$, the ring ratio becomes the ratio of effective efficiencies averaged over the neutron spectrum:

$$\frac{O}{I} = \frac{\epsilon_O^{\text{eff}}}{\epsilon_I^{\text{eff}}}. \tag{3}$$

We now wish to determine how the observed ring ratio [Eq. (3)] is related to the true average energy E_{av} defined as

$$E_{av} = \frac{\int N(E)E\,dE}{\int N(E)\,dE}. \tag{4}$$

We have done this in an empirical manner by calculating average energies and effective efficiencies for each ring for all the nuclides measured here and for which spectra are available from the work of Shalev and Rudstam.[8,12,13,14] The average energy was obtained by reading the intensity $N(E)$ of the published spectra at about 20 keV intervals and calculating E_{av} from $\sum N(E)E/\sum N(E)$. The effective efficiency was obtained in a similar

manner by calculating ϵ^{eff} from $\sum N(E)\epsilon(E)/\sum N(E)$.

The resulting effective ring ratios versus average energies are shown in Fig. 5 as closed points without error bars. From 250 to 550 keV the effective ring ratios are close to the values for a monoenergetic source, but they deviate considerably above this range. This may be related to the fact that a delayed-neutron spectrum with an average energy greater than 550 keV has appreciable numbers of neutrons greater than 800 keV. Above 800 keV the absolute efficiency curves for all three rings are decreasing with energy and the ring ratio is no longer a sensitive measure of the neutron energy. Consequently the detailed shape of the neutron spectrum becomes increasingly significant in determining effective ring ratios and average energies as the average energy increases above 550 keV.

The points in Fig. 5 at 585 and 608 keV are for the ^{135}Sb and ^{85}As spectra, respectively, which were measured by Shalev and Rudstam but were not measured in the present work. These two spectra were also measured by Franz *et al.*[9] and the corresponding data points are shown at 793 and 650 keV for ^{135}Sb and ^{85}As, respectively. The data points at 750 keV refer to the Franz *et al.* spectrum of ^{135}Sb but are integrated only over the same energy region as shown by Shalev and Rudstam. Since different values of the average energy are obtained for the same spectrum as measured by different authors, there is some uncertainty in the corrected calibration curve particularly above 550 keV. We have adopted the corrected calibration curve shown as the dashed line in Fig. 5 in the region from 250 to 600 keV. Above this energy range we have adopted the solid curve as a lower limit to the average energy for a given ring ratio.

There is an additional uncertainty in the corrected calibration curve due to the fact that the Shalev and Rudstam spectra do not extend below about

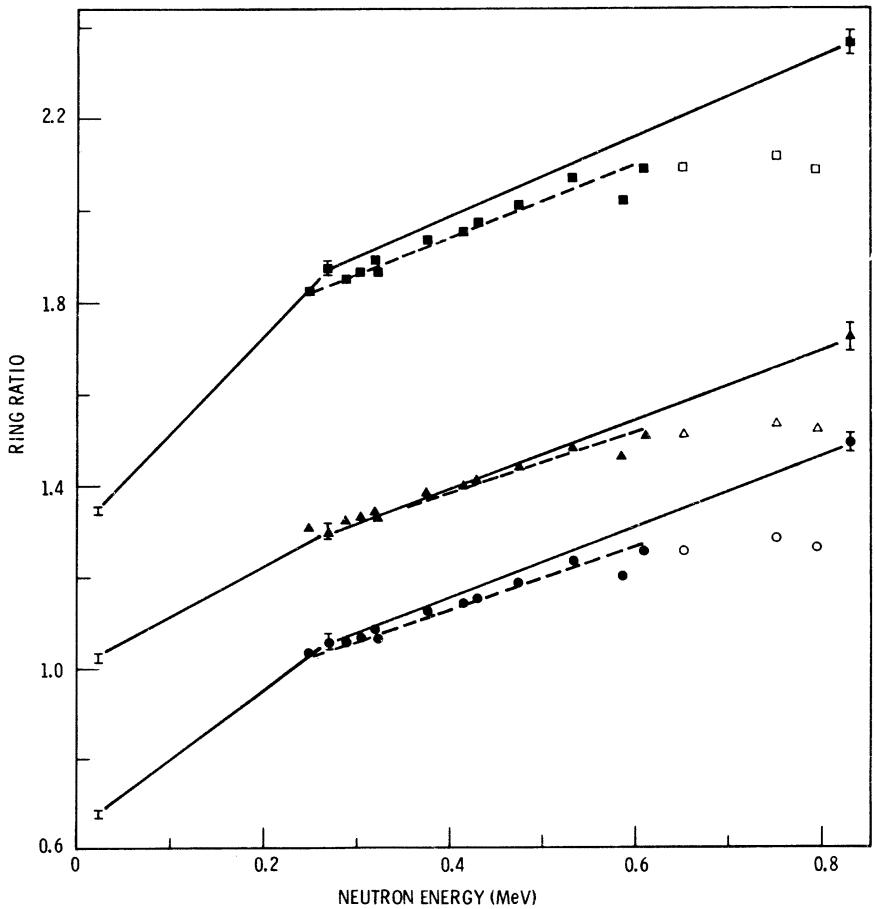

FIG. 5. Ring ratio versus neutron energy: Circles denote outer/inner; triangles denote outer/middle, and squares denote outer+middle/inner. Points with error bars are measured for monoenergetic sources. Closed points without error bars are effective ring ratio versus average neutron energy calculated from spectra of Shalev and Rudstam. Open points are similar data from spectra of Franz *et al.*

TABLE II. Typical neutron background counting rates (counts/sec) with baffle in place.

	Cosmic ray and noise	Reactor	Kr, Xe	Total
Inner	0.13	0.27	0.22	0.62
Middle	0.12	0.22	0.11	0.45
Outer	0.26	0.62	0.08	0.96
Total	0.51	1.11	0.41	2.03

100 keV. However, inclusion of neutrons below 100 keV lowers both the average energy of a given spectrum and the effective ring ratio so that the location of the corrected calibration curve is only slightly affected.

E. Neutron backgrounds

With the SNC in position on the SOLAR beam pipe, the neutron background was investigated under various running conditions to determine the source of background neutrons. The background increased when the reactor was turned on due to the neutrons from the reactor which penetrated the counter shielding. However, the background also increased when the target oven was heated and the Cd shutter around the target was opened—even though the ion acceleration voltage was off. This effect was attributed to delayed neutrons from neutral gaseous fission products (Kr, Xe) which diffused out of the target and drifted inside the beam tube out to the vicinity of the SNC. The neutron count rate due to these neutral fission products varies with the temperature of the oven and dominated the over-all background. However, the background from this effect was reduced by a factor of 10 by placing a baffle with a 4.8 mm high by 1.3 mm wide slit for the ion beam at the beginning of the beam pipe extension. Typical background rates identified according to the source of the neutrons are given in Table II for each ring.

F. Data collection

Most of the ring ratio measurements were performed in conjunction with P_n experiments described in the following paper.[1] These experiments involved repetitive cycles of intermittent ion beam collection on the first dynode of the electron multiplier. Neutron counts were accumulated continuously in two or three scalers depending on how the rings were being monitored. Delayed-neutron emission rates depended on the ion beam intensity at a particular mass and on the delayed-neutron emission probability of the particular precursor. The maximum emission rate obtained in this work was 7000 n/sec for ^{94}Rb which corresponded to a neutron count rate of 2700 cps. Some of the data reported here are based on net count rates as low as 2 cps for cases in which the beam intensities or P_n values were low. Neutron backgrounds were measured with 100 sec runs taken immediately before and after each run. No variation of neutron background was observed as long as the temperature of the oven remained constant. Therefore all background runs taken at the same temperature were combined to increase the statistical accuracy.

One set of experiments was run specifically to get ring ratio measurements on all Rb and Cs isotopes on the same day under identical conditions. These experiments consisted of continuous deposition of the desired nuclide with simultaneous counting of neutrons from each ring separately. This procedure gave faster data collection rates than for the pulsed beam experiments, but the results were equivalent. The ring ratio data and corresponding energies for this particular set of experiments are shown in Table III.

G. Data analysis

The data were analyzed separately for those cases where each ring was scaled individually (method A) and for those cases where the middle and outer rings were scaled together (method B). In method A, ring ratios of outer/inner, outer/middle, and outer-plus-middle/inner were calculated from the scaler counts after correction for

TABLE III. Ring ratios for Rb and Cs nuclides for one set of experiments having continuous deposition of ion beam. Corresponding average neutron energies (MeV) are given in parentheses.

Mass	O/I	O/M	O+M/I
93	1.23 ± 0.02 (0.53 ± 0.03)	1.50 ± 0.03 (0.56 ± 0.04)	2.06 ± 0.03 (0.54 ± 0.04)
94	1.23 ± 0.02 (0.53 ± 0.03)	1.49 ± 0.02 (0.55 ± 0.03)	2.05 ± 0.02 (0.53 ± 0.03)
95	1.26 ± 0.03 (0.58 ± 0.03)	1.45 ± 0.03 (0.49 ± 0.04)	2.13 ± 0.04 (0.62 ± 0.05)
96	1.23 ± 0.03 (0.53 ± 0.04)	1.46 ± 0.04 (0.50 ± 0.06)	2.07 ± 0.05 (0.55 ± 0.06)
97	1.42 ± 0.06 (>0.73)	1.55 ± 0.06 (>0.60)	2.34 ± 0.08 (>0.80)
143	1.09 ± 0.03 (0.34 ± 0.04)	1.38 ± 0.04 (0.39 ± 0.06)	1.89 ± 0.04 (0.33 ± 0.05)
144	1.04 ± 0.03 (0.27 ± 0.04)	1.34 ± 0.04 (0.33 ± 0.06)	1.81 ± 0.05 (0.24 ± 0.05)
145	1.20 ± 0.07 (0.49 ± 0.10)	1.46 ± 0.08 (0.50 ± 0.11)	2.03 ± 0.10 (0.50 ± 0.12)

TABLE IV. Average energy (MeV) of delayed neutrons. The uncertainty shown does not include systematic uncertainty due to calibration curve. The numbers in parentheses are the number of runs included to obtain average ring ratio.

Element	Mass	SOLAR Method A	SOLAR Method B	Shalev and Rudstam[a]
Br	87		0.15 ± 0.01 (4)	0.25
	88		0.33 ± 0.03 (3)	0.30
	89		>0.71 (2)	0.47
Rb	92	0.18 ± 0.04 (4)	0.12 ± 0.03 (1)	
	93	0.56 ± 0.01 (4)	0.63 ± 0.01 (5)	0.38
	94	0.57 ± 0.01 (6)	0.61 ± 0.01 (9)	0.42
	95	0.53 ± 0.01 (6)	0.57 ± 0.01 (5)	0.43
	96	0.56 ± 0.01 (6)	0.54 ± 0.01 (5)	
	97	>0.72 (3)	>0.62 (2)	
I	137		0.53 ± 0.05 (2)	0.53
Cs	141		0.24 ± 0.05 (1)	
	142	0.24 ± 0.06 (2)	0.13 ± 0.01 (4)	0.32
	143	0.35 ± 0.01 (6)	0.32 ± 0.02 (6)	0.29
	144	0.29 ± 0.02 (4)	0.33 ± 0.02 (6)	0.32
	145	0.46 ± 0.03 (4)	0.54 ± 0.02 (6)	
	146		0.53 ± 0.07 (2)	

[a]References 8, 12, 13, and 14. Upper limit calculated as described in Sec. II D.

backgrounds. In some runs, the ring ratios were perturbed when pulses from one of the rings were simultaneously sent to the 100-channel analyzer to monitor the pulse height. However, this effect could easily be corrected by factors determined from similar runs with ^{94}Rb or the RaBe source. In a few runs, the inner ring was not used, so only the outer/middle ratio was calculated. The data from all runs were combined to give weighted averages of each of the three ring ratios. The ring ratios were then compared with the calibration curves in Fig. 5 to give three values for the average energy. These three energies were then combined to give a weighted average value for the average neutron energy of the delayed-neutron spectrum. These energies are listed under method A in Table IV.

In method B, only one ring ratio was available, outer-plus-middle/inner (OM/I). It was noted that on particular days, these ratios were consistently lower than the same ratios from method A. The cause of this discrepancy was not identified. In order to use method B data to get average energies for a number of nuclides for which no method A data were available, it was necessary to determine correction factors. For a set of runs taken on the same day, the weighted average method A OM/I ratio was divided by the method B OM/I ratio. These ratios for different nuclides measured on the same day were averaged to give a correction factor for that particular day. Most of the data of this type was taken over a one-month period during which the correction factor was constant at 1.286 ±0.004. For each nuclide, all the OM/I data from corrected method B ratios were combined to give a weighted average OM/I ratio. This value was then converted to an average neutron energy using the calibration curve of Fig. 5. These energies are listed under method B in Table IV.

The errors given in Table IV represent the energy spread due to the uncertainties of the weighted average ring ratios. The ring ratio uncertainties take into account only the statistical accuracy of the counting data and background measurements. Any systematic error due to the calibration curve is not included in the errors shown.

III. DISCUSSION

A. Individual precursors

The average energies determined here may be compared with average energies based on the published spectra of Shalev and Rudstam.[8,12-14] The calculations discussed in Sec. II D assumed zero intensity below 100 keV and thus gave only upper limits to the average energies. These upper limits to E_{av} are given in Table IV along with the present results. The uncertainties on the upper limit estimates are difficult to determine since they are not based on the detailed original data and since peaks of the order of 20 keV wide are present in the original data. However, a reasonable estimate of the uncertainties might be ±0.03 MeV.

Comparison of the present E_{av} data with the upper limits of E_{av} based on Shalev and Rudstam's spectra shows two cases (^{87}Br and ^{142}Cs) where the

present results give considerably lower average energies. This indicates that the ^{87}Br and ^{142}Cs spectra probably have important contributions from neutrons below 100 keV. The average energies obtained here for ^{88}Br, ^{137}I, ^{143}Cs, and ^{144}Cs are in reasonable agreement with the upper limits from Shalev and Rudstam's work; however, the present results for ^{89}Br, ^{93}Rb, ^{94}Rb, and ^{95}Rb are significantly higher than the values obtained from Shalev and Rudstam's spectra. This is difficult to explain without invoking an error in the calibration curve used here or an error in the response functions used by Shalev and Rudstam. It should be noted that the ^{135}Sb spectrum of Franz *et al.*[9] gives a significantly higher average energy (0.79 MeV) than the ^{135}Sb spectrum of Shalev and Rudstam[8] (0.59 MeV).

The average energies measured here and the upper limits from the Shalev and Rudstam spectra both show strong variations from one nuclide to another. For a theoretical understanding of these variations, one can write the following expression for the average energy of the delayed neutrons,[8,15,23]

$$E_{av} = \frac{\int_{B_n}^{Q_\beta} f(Z+1, Q_\beta - E) S_\beta(E) E_n \, dE}{\int_{B_n}^{Q_\beta} f(Z+1, Q_\beta - E) S_\beta(E) \, dE} , \quad (5)$$

where Q_β is the total energy available in β^- decay of the precursor (Z, N), B_n is the neutron binding energy in the emitter $(Z+1, N-1)$, E is the excitation energy of the emitter, $f(Z+1, Q_\beta - E)$ is the statistical rate function (Fermi function), $S_\beta(E)$ is the β^- strength function defined as the product of the level density and the average of the squares of the nuclear matrix elements, and E_n is the energy of the emitted neutron.

The expression for E_{av} is greatly simplified with the following assumptions:

$$f(Z+1, Q_\beta - E) = \text{const.}\ (Q_\beta - E)^5 ,$$

$$S_\beta = \text{const.} ,$$

$$E_n = E - B_n .$$

With these assumptions, E_{av} becomes

$$E_{av} = \frac{\int_{B_n}^{Q_\beta} (Q_\beta - E)^5 (E - B_n) \, dE}{\int_{B_n}^{Q_\beta} (Q_\beta - E)^5 \, dE} , \quad (6)$$

$$E_{av} = \tfrac{1}{7} (Q_\beta - B_n) . \quad (7)$$

In Table V, our experimental data are compared with values calculated from Eq. (7) for two different semiempirical mass tables.[24,25] The SOLAR method A values have been adopted in Table V whenever possible.

The simple expression Eq. (7) predicts general trends, but is not adequate for detailed comparisons. The quantity $Q_\beta - B_n$ is commonly called the neutron window. Different mass formulas generally give similar values for this quantity, but it obviously would be better to use experimental values for the neutron window, if available. Previous workers have noted that for neutron excess nuclides the assumption of a constant β strength function is not valid.[8,26] A steeply rising β strength function could explain why certain experimental values of the average delayed-neutron energy are higher than the predicted values. The simple expression Eq. (7) also neglects γ competition from energy levels slightly above the neutron binding energy. This effect would reduce the number of neutrons emitted at low energies and hence would give a delayed-neutron spectrum with a somewhat higher average energy. On the other hand, neutron emission to excited states of the final nucleus would give average energies lower than those predicted by Eq. (7).

TABLE V. Comparison of experimental (SOLAR) and calculated average delayed-neutron energies (MeV).

Element	Mass	SOLAR	Garvey *et al.*[a]	Myers[b]
Br	87	0.15 ± 0.01	0.17	0.19
	88	0.33 ± 0.03	0.26	0.27
	89	>0.71	0.40	0.41
Rb	92	0.18 ± 0.04	0.06	0.05
	93	0.56 ± 0.01	0.21	0.14
	94	0.57 ± 0.01	0.33	0.15
	95	0.53 ± 0.01	0.46	0.27
	96	0.56 ± 0.01	0.59	0.35
	97	>0.72	0.73	0.49
I	137	0.53 ± 0.05	0.19	0.22
Cs	141	0.24 ± 0.05	0.05	0.05
	142	0.24 ± 0.06	0.15	0.11
	143	0.35 ± 0.01	0.23	0.20
	144	0.29 ± 0.02	0.27	0.25
	145	0.46 ± 0.03	0.32	0.35
	146	0.53 ± 0.07	0.30	0.39

[a]Reference 24. [b]Reference 25.

B. Delayed-neutron groups

For calculations of the kinetic behavior of reactors, the delayed-neutron precursors are commonly approximated by six groups, each with an effective half-life and effective abundance.[27] Previous experimenters have measured the energy spectra associated with each of the four or five longer-lived groups and have reported average energies for these groups.[4,28-30]

The average neutron energies for each group can be calculated from data on individual precursors provided the delayed-neutron yield of each precursor is known. For the system ^{235}U plus

TABLE VI. Average energies (MeV) of delayed-neutron groups in thermal neutron fission of ^{235}U.

Measurement Group	1	2	3	4	5	6
This work[a]	0.15 (100)	0.46 (97)	>0.6? (74)	0.54 (34)	0.52 (26)	>0.61 (81)
Fieg[b]	0.28 ± 0.03	0.48 ± 0.05	0.45 ± 0.05	0.43 ± 0.04		
Batchelor and Hyder[c]	0.25 ± 0.02	0.46 ± 0.01	0.41 ± 0.02	0.45 ± 0.02		
Burgy *et al.*[d]	0.30 ± 0.06	0.67 ± 0.01	0.65 ± 0.09	0.91 ± 0.09	0.40 ± 0.07	
Hughes *et al.*[e]	0.25 ± 0.06	0.56 ± 0.06	0.43 ± 0.06	0.62 ± 0.06	0.42 ± 0.06	

[a] The numbers in parentheses are the percent of the total group yield included in our calculation.
[b] Reference 4.
[c] Reference 28.
[d] Reference 29.
[e] Reference 30.

thermal neutrons, Izak-Biran and Amiel[31] have calculated the delayed-neutron yield of individual precursors from cumulative fission yields and recent values of the delayed neutron emission probabilities (P_n). The precursors reported here account for most of the delayed neutron yield in four of the six groups. We have calculated average neutron energies for each group by weighting our measured average energies for individual precursors by the delayed-neutron yields (DNY) given by Izak-Biran and Amiel and combining all members of a particular group as shown in the following equation:

$$E_{av}(\text{group}) = \frac{\sum_i (\text{DNY})_i (E_{av})_i}{\sum_i (\text{DNY})_i} . \quad (8)$$

The sum is over the i precursors of a particular group for which average energies were measured here. We also calculated the fraction of the total group yield included in the above sum. These results are shown in Table VI along with the earlier values of the average neutron energies.

There is a clear discrepancy between the average energy measured here for ^{87}Br and the average energy of group 1 (100% ^{87}Br) measured previously. However, the earlier work was not sensitive to neutrons below 100 keV. Chrysochoides *et al.*[10] report the presence of neutron peaks at 45, 70, and 110 keV in the time of flight spectrum of ^{87}Br. Intense peaks at similar energies were seen in the gross spectra of Sloan and Woodruff.[5] Ray and Kenney[32] have recently measured the ^{87}Br neutron spectrum above 100 keV with a proton recoil detector and report a considerably softer spectrum than that given by Shalev and Rudstam. These data support the lower average energy for group 1 reported here.

The delayed-neutron yields calculated by Izak-Biran and Amiel account for all of the experimentally measured group yields. It is not likely that undiscovered delayed-neutron emitters will alter the present data. However, it should be noted that the present data on group 4 and group 5 precursors represent only $\frac{1}{3}$ and $\frac{1}{4}$ of the group yields.

IV. SUMMARY AND CONCLUSIONS

We have described an experimental method for obtaining average energies of delayed-neutron spectra from chemically and mass separated sources. The method based on counting rate ratios of rings of neutron counter tubes in a block of polyethylene allows measurements both on nuclides with very low P_n and on nuclides with very low fission yield. Significant variations of the average neutron energy have been found among the 16 nuclides reported here. A simple expression [Eq. (7)] qualitatively predicts the average energy. Quantitative predictions, however, require far more elaborate expressions containing many more parameters—some of which are highly uncertain at this time.

Average energies of all six delayed-neutron groups used in reactor kinetics calculations were calculated from the data on individual precursors. The group 1 energy is significantly lower than the previous measurements, but earlier techniques were not sensitive to neutrons below 100 keV.

ACKNOWLEDGMENTS

We wish to acknowledge W. Wilson, T. Lovas, and the reactor operators at Washington State University for their cooperation and assistance to the SOLAR project. Professor J. Lin of Tennessee Technological University assisted in some of the neutron counter calibration work as a Northwest College and University Association for Science Summer Fellow. The Hanford precision long counter H4 was loaned to us by L. L. Nichols who also assisted in the calibration of the Washington State University ^{252}Cf source.

*Work performed under ERDA, Contract No. EY-76-C-06-1830.

†Present address: Los Alamos Scientific Laboratory, University of California, Los Alamos, New Mexico 87544.

[1]P. L. Reeder, J. F. Wright, and L. J. Alquist, following paper, Phys. Rev. C 15, 2108 (1977).

[2]S. Yiftah and D. Saphier, in *Delayed Fission Neutrons* (International Atomic Energy Agency, Vienna, 1968), p. 23. Also in Trans. Am. Nucl. Soc. 11, 568 (1968).

[3]G. R. Keepin, in *Delayed Fission Neutrons* (International Atomic Energy Agency, Vienna, 1968), p. 3.

[4]G. Fieg, J. Nucl. Energy 26, 585 (1972).

[5]W. R. Sloan and G. L. Woodruff, Nucl. Sci. Eng. 55, 28 (1974).

[6]S. Shalev and J. M. Cuttler, Nucl. Sci. Eng. 51, 52 (1972).

[7]A. E. Evans and L. V. East, Trans. Am. Nucl. Soc. 19, 396 (1974).

[8]S. Shalev and G. Rudstam, Nucl. Phys. A230, 153 (1974).

[9]H. Franz, J. V. Kratz, K. L. Kratz, W. Rudolph, G. Herrmann, F. M. Nuh, S. G. Prussin, and A. A. Shihab-Eldin, Phys. Rev. Lett. 33, 859 (1974).

[10]N. G. Chrysochoides, J. N. Anouss, C. A. Mitsonias, and D. C. Perricos, J. Nucl. Energy 25, 551 (1971).

[11]J. Norman, Ph.D. thesis, Iowa State University, 1973 (unpublished).

[12]G. Rudstam and S. Shalev, Nucl. Phys. A235, 397 (1974).

[13]G. Rudstam, S. Shalev, and O. C. Jonsson, Nucl. Instrum. Methods 120, 333 (1974).

[14]S. Shalev and G. Rudstam, The Swedish Research Council's Laboratory, Studsvik, Report No. LF-64, 1975 (unpublished).

[15]K. Takahashi, Progr. Theor. Phys. 47, 1500 (1972).

[16]J. J. Stoffels, Nucl. Instrum. Methods 119, 251 (1974).

[17]The ^{3}He counter tubes were kindly loaned to us by Dr. O. K. Harling.

[18]The Hanford standard PuBe source M1221 was calibrated to an accuracy of 1% by the National Bureau of Standards in 1973.

[19]J. DePangher and L. L. Nichols, Battelle, Pacific Northwest Laboratories, Report No. BNWL-260, 1966 (unpublished).

[20]T. R. Hill, Los Alamos Scientific Laboratory, Report No. LA-5990-MS, 1975 (unpublished).

[21]J. F. Wright, L. J. Alquist, J. Lin, and P. L. Reeder, Bull. Am. Phys. Soc. 21, 1007 (1976).

[22]L. V. East and R. B. Walton, Nucl. Instrum. Methods 72, 161 (1969).

[23]K. L. Kratz and G. Herrmann, Nucl. Phys. A229, 179 (1974).

[24]G. T. Garvey, W. J. Gerace, R. L. Jaffe, I. Talmi, and I. Kelson, Rev. Mod. Phys. 41, S1 (1969).

[25]W. D. Myers, Lawrence Berkeley Laboratory, Report No. LBL-3428, 1974 (unpublished).

[26]K. Aleklett, G. Nyman, and G. Rudstam, Nucl. Phys. A246, 425 (1975).

[27]R. J. Tuttle, Nucl. Sci. Eng. 56, 37 (1975).

[28]R. Batchelor and M. R. McK. Hyder, J. Nucl. Energy 3, 7 (1956).

[29]M. Burgy, L. A. Pardue, H. B. Willard, and E. O. Wollan, Phys. Rev. 70, 104 (1946).

[30]D. J. Hughes, J. Dabbs, A. Cahn, and D. Hall, Phys. Rev. 73, 111 (1948).

[31]T. Izak-Biran and S. Amiel, Nucl. Sci. Eng. 57, 117 (1975).

[32]P. K. Ray and E. S. Kenney, Nucl. Instrum. Methods 134, 559 (1976).